ACS OMEGA

http://pubs.acs.org/journal/acsodf

Article

Probing Charge Transport Kinetics in a Plasmonic Environment with Cyclic Voltammetry

Mohammad Shahabuddin,* Ashleigh K. Wilson, Ashah C. Koech, and Natalia Noginova

Cite This: *ACS Omega* 2021, 6, 34294–34300

Read Online

ACCESS | Metrics & More | Article Recommendations

ABSTRACT: Possible modifications in electrochemical reaction kinetics are explored in a nanostructured plasmonic environment with and without additional light illumination using a cyclic voltammetry (CV) method. In nanostructured gold, the effect of light on anodic and cathodic currents is much pronounced than that in a flat system. The electron-transfer rate shows a 3-fold increase under photoexcitation. The findings indicate a possibility of using plasmonic excitations for controlling electrochemical reactions.

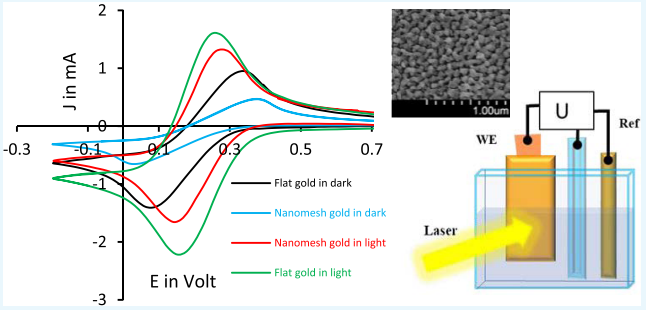

INTRODUCTION

Plasmonic metamaterials and metasurfaces can provide unprecedented control of light[1−3] and bring new possibilities for modifying and controlling various physical and chemical phenomena. The range of such phenomena is very broad, including strong modifications in the spontaneous emission rate and spectrum,[4−10] change in the Förster energy transfer rate,[11,12] modification of van der Waals forces, and new or accelerated chemical reactions[13−18] in the vicinity of plasmonic structures, metasurfaces, and metamaterials. The mechanisms of these effects are often related to the modified density of photonic modes, which can be very significant (reaching infinity in hyperbolic metamaterials).[2,19−21] However, depending on the process, other factors can play a defining role. These factors are also specific for nanostructured or/and plasmonic media, such as enhanced roles of surface and surface effects, charging of nanofeatures,[22,23] or emission of hot electrons[24−29] under plasmon resonance conditions.

Recently, it was found that the charge-transfer process and charge transport kinetics can be significantly altered in a plasmonic environment.[13,30−37] In experiments with electrochromic polymers such as polyaniline (PANI)[38−40] and Prussian blue,[41] acceleration of the color switching and high color contrast have been demonstrated in plasmonic cavities, single-slit waveguides, and gold nanomesh substrates. In refs 39, 42, PANI deposited on the plasmonic gold nanomesh substrate demonstrates the behavior significantly different from that in flat gold: a very steep color switching is observed at a small increment of the voltage over some threshold value, and an additional peak is recorded in the cyclic voltammetry curves. These effects are tentatively ascribed to a possible interface-related charging and Schottky barrier formation;[39] however, the full picture of the observed effects is not yet fully clear.

Studies of electrochemical reactions in a plasmonic environment are still at the initial stage, and more experiments are needed to explore opportunities for controlling or modifying this process with plasmonic systems and metamaterials. Note that charge transport in the electrochromic reactions of PANI is rather complicated due to its multistep process with varied voltage; therefore, in this case, identifying plasmonic-related effects involved in the modification of the heterogeneous charge-transfer process is complicated. In this work, we consider a much simpler process: a single-electron-transfer oxidation−reduction reaction of hexacyanoferrite iron(II) state to hexacyanoferrate iron(III) state in the K_3 $Fe(CN)_6$/KNO_3 aqueous media.

$$\text{oxidation, } O_1 \quad \overset{k^f}{\underset{k^r}{\rightleftarrows}} \quad \text{reduction, } R_1$$

$$[Fe(CN)_6]^{4-} \rightleftarrows [Fe(CN)_6]^{3-} + e^-$$

$$\text{iron(II) state} \rightleftarrows \text{iron(III) state} + e^-$$

In the current work, we investigate how the vicinity to a nanostructured metallic surface affects this single electron-

Received: July 16, 2021
Accepted: October 4, 2021
Published: December 10, 2021

https://doi.org/10.1021/acsomega.1c03794
ACS Omega 2021, 6, 34294−34300

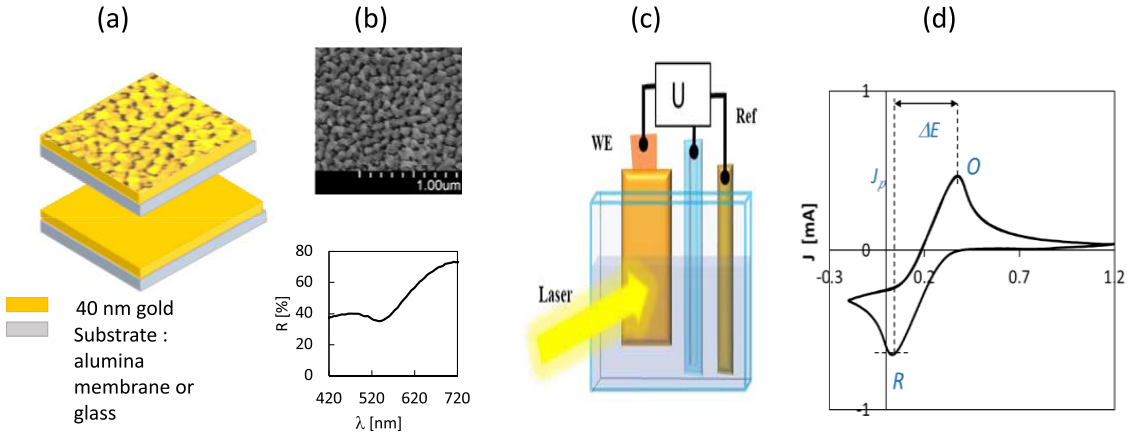

Figure 1. (a) Schematic of the gold nanomesh and flat gold substrate; (b) SEM (top) and the reflection spectrum (bottom) of nanomesh (taken from the sample in the electrolyte); (c) schematic of the experimental setup; and (d) typical cyclic voltammogram of iron(II) to (III) exchange in $K_3[Fe(CN)_6]/KNO_3$ aqueous media with the potentiodynamic sweep (flat gold, 60 mV/s, dark field).

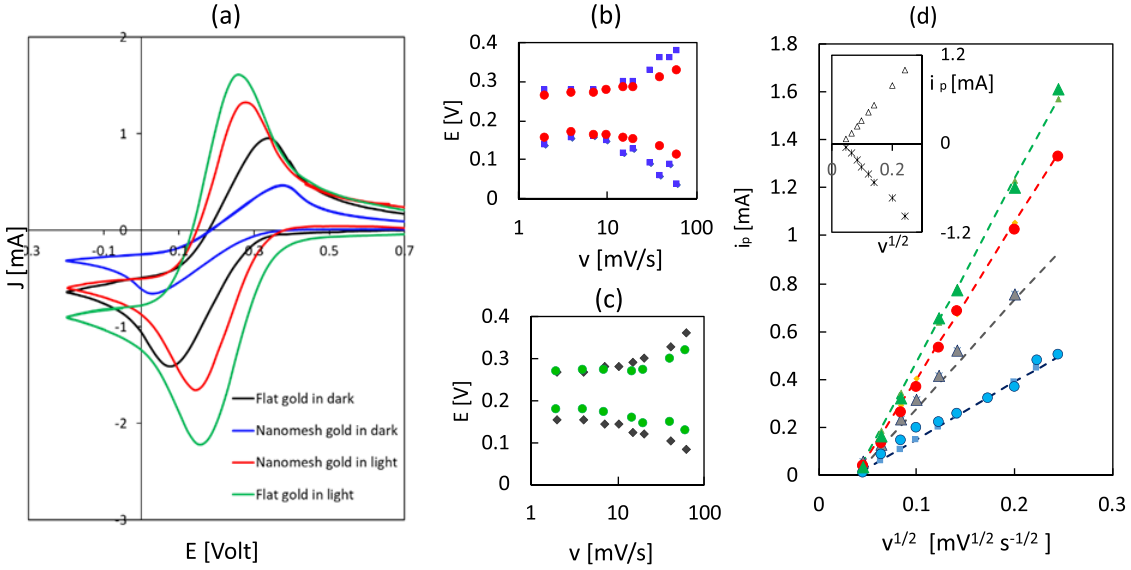

Figure 2. (a) Cyclic voltammogram obtained using flat gold (in light and dark fields) and nanomesh gold (in light and dark fields) as working electrodes. Scan rate is shown for each electrode, 60 mV/s. (b) Oxidation−reduction peak potential in nanomesh vs v sweep rate in light and dark; (c) same in flat gold; and (d) anodic peak current vs $v^{1/2}$, experiment (points) and fitting (dashed traces). Inset: anodic (triangles) and cathodic (stars) currents in flat gold in dark.

transfer process and modifies the charge transport kinetics. We use the same type of nanostructured environment that had been used in previous experiments with PANI.[39] Similar to previous work done, we employ the cyclic voltammetry (CV) method and perform a comparative study of the reaction using two different electrodes, flat gold and gold nanomesh. In addition, we explore the possible effects of laser light illumination. The CV data will be used to analyze the kinetics of the reaction, specifically the heterogeneous electron-transfer rate (HET), which characterizes the electron transfer between electroactive species and an electrode surface. The information acquired on the kinetics of heterogeneous electron transfer for different types of the electrode surface and the possibility to control or modify this process is of great importance for various applications.

EXPERIMENTAL SECTION

The schematics of nanoporous and flat gold electrodes are shown in Figure 1a. Glass and nanoporous anodic aluminum oxide (AAO) substrates (with a pore diameter of about 40 nm) are precleaned and precoated with an adhesion layer of 3 nm thick Cr. Gold with a thickness of 40 nm is deposited with the thermal evaporation method. The deposition of gold onto the AAO substrate produces highly nanostructured surfaces, with optical properties mainly defined by plasmonic resonances that are observed as a broad dip in transmission[39] or reflection spectra around λ = 548 nm, Figure 1b.

The experimental setup is shown in Figure 1c. A transparent quartz cuvette with dimensions of 30 mm × 20 mm × 10 mm is filled by two-thirds with the $K_3Fe(CN)_6$ electrolyte solution. The solution is prepared from distilled water, 100 mM $K_3Fe(CN)_6$ (99.99%, Scientific Fisher), and 1 M KNO_3 (99.99%, Sigma-Aldrich).

The CV data are collected with a Biologic SP-300 potentiostat, employing a standard three-electrode system: (1) the flat gold or gold nanomesh substrate under study (with the surface area of about 0.2 cm^2) is used as the working electrode, (2) a saturated Ag/AgCl calomel electrode as the reference electrode, and (3) a platinum wire with the diameter of 1 mm

https://doi.org/10.1021/acsomega.1c03794
ACS Omega 2021, 6, 34294−34300

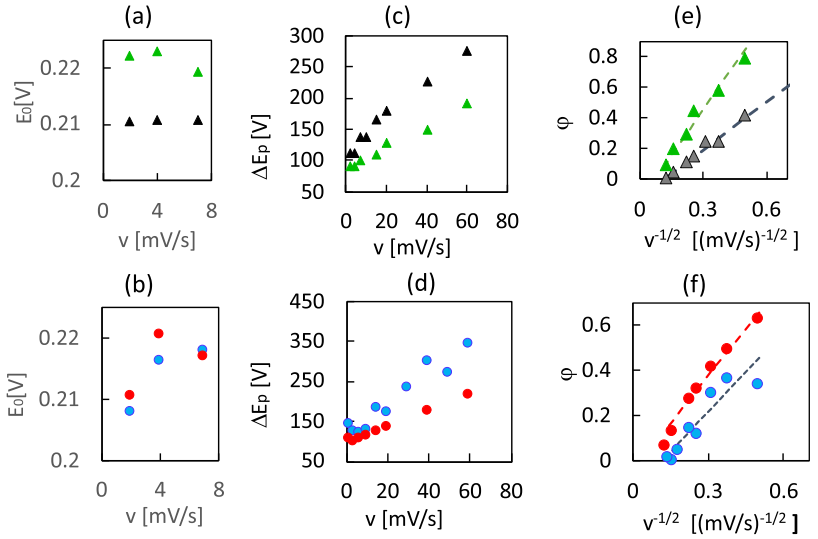

Figure 3. Redox potential (a, b), peak-to-peak separation (c, d), and Nicholson kinetic parameter (e, f) in flat gold (top three plots) and nanomesh systems (three bottom plots). Red and green colors correspond to the data obtained under light illumination, and blue and black data are obtained in dark. Dashed traces in (e) and (f) are fitting with straight lines.

serves as the counter electrode. A typical CV curve observed in our experiments, Figure 1d, exhibits a pair of well-defined redox peaks and with peak-to-peak separations. The ΔE of 190.4 mv at 60 mV/s in flat gold agrees with prior literature.[43−45]

The experiments are performed without and with additional light illumination, referred to as "in dark" and "in light," respectively. The additional illumination is provided by a diode laser with the wavelength 585 nm and 100 mW power. Light is focused on the submerged area (5 mm × 5 mm) of the working electrode, which is our sample under study (gold nanomesh or flat gold depending on a particular run), resulting in the illumination intensity of 400 mW/cm^2. To ensure that light illumination does not induce an irreversible reaction, CV curves are first taken in dark and then are repeated in dark again after the exposure to light; they practically coincide with the curves recorded before the exposure.

RESULTS AND DISCUSSION

The CV curves are recorded for various sweeping rates, v, ranging from 1 to 100 mV/s by sweeping the potential between −0.2 and 1.2 V. Each experimental run is repeated for different types of the substrate (flat or nanostructured) in dark and light fields. Examples shown in Figure 2a correspond to four different cases denoted with different colors: flat gold in dark (black), flat gold with light (green), gold nanomesh in dark (blue), and gold nanomesh with light (red). The same color scheme is used in all Figures 2 and 3 subplots as well.

The effects of the nanostructured environment and light are clearly seen in Figure 2. Under light illumination, currents are higher than in dark, and the change in the current is stronger in nanostructured gold than that in flat (compare green and black traces for flat gold with blue and red for the nanostructure). Positions of oxidation and reduction peaks change as well: the peak separation, ΔE, becomes lower. The effects of light are apparently more pronounced in the nanostructured system than in flat gold.

The dependence of oxidation and reduction peak positions on sweep rate, v, in the flat and nanostructured systems are shown correspondingly in Figure 2b,c. With increasing in the scan rate, the reduction peak moves toward higher negative potential while the oxidation peak shifts toward higher positive potential as expected.

The anodic and cathodic peak currents (measured, respectively, at the oxidation and reduction peak positions) are of the opposite polarity and have the same magnitude (confirming the reversibility of the process), see the example in the inset of Figure 2d. The magnitude of the peaks increases with the increasing rate. It is instructive to plot their magnitude as the function of the square root of the sweep rate (Randles−Sevcik's plot[46,47]), Figure 2d, which clearly shows the predominating term, $\alpha v^{1/2}$, where α is the coefficient of proportionality. This dependence and equal magnitude of anodic and cathodic currents indicate that the redox couple $K_3Fe(CN)_6$ behaves reversibly under the diffusion-controlled process described with the Randles−Sevcik's equation,[47]

$$i_p = (0.4463(nF)^{3/2})A\sqrt{\frac{D}{RT}}Cv^{1/2} \quad (1)$$

where i_p is the peak current (in amps), D is the diffusion coefficient in cm^2/s, F = 96485 C/mol is the Faraday constant, n is the number of electrons (n = 1 for a single-electron process), A is the electrode surface area (cm^2), C is the analyte concentration (mol/cm), R = 8.31446 J/(K mol) is the gas constant, v is in V/s, and T is the temperature.In the analysis, we take into account the data obtained in three different trials and fit the dependence of the peak current vs rate with the following slopes:

- For the flat electrode in dark and light, respectively: α_{dark}^{flat} = 4.7 ± 0.2 mA/(mV$^{1/2}$ s$^{-1/2}$), α_{light}^{flat} = 7.6 ± 0.2 mA/(mV$^{1/2}$ s$^{-1/2}$)
- For nanomesh: α_{dark}^{nano} = 2.4 ± 0.1 mA/(mV$^{1/2}$ s$^{-1/2}$) and α_{light}^{nano} = 6.5 ± 0.2 mA/(mV$^{1/2}$ s$^{-1/2}$)

A 2-fold difference is observed between dark values for the flat and nanostructured systems. Assuming that other parameters are the same in both cases, it can be ascribed to the difference in the effective surface area: the working area in the nanomesh electrode is less than that in the flat gold of the same size, due to the porous structure of our nanostructure ("filling factor" of nanomesh of around 50%[23,48]).

https://doi.org/10.1021/acsomega.1c03794
ACS Omega 2021, 6, 34294−34300

The light-induced changes in slopes are much stronger in the nanostructured system.

$$\frac{\alpha_{light}^{flat}}{\alpha_{dark}^{flat}} = 1.62 \pm 0.1 \quad (2a)$$

$$\frac{\alpha_{light}^{nano}}{\alpha_{dark}^{nano}} = 2.71 \pm 0.1 \quad (2b)$$

Let us now analyze the position of the peaks, their shift as the function of the sweep rate, and the effect of light illumination. At low rates, the oxidation and reduction peaks are well-defined, and their positions stay practically unchanged. We use the data at low v to estimate the standard electrode potential, as the average between the positions of oxidation, E_{ox}, and reduction, E_r, peaks, $E_0 = 1/2(E_{ox} + E_r)$, see Figure 3a,b. Under illumination, E_0 slightly increases for both substrates.

The peak-to-peak separation, ΔE_p, is an important factor, which can be used for characterizing the performance of an electrode material and estimating HET rates. Generally, low values of ΔE correspond to reversible reactions with fast reaction kinetics. The electrochemical response of our electrodes presented in Figure 3c,d reveals relatively large ΔE_p, indicating slow and unfavorable HET kinetics. The values of ΔE_p increase with the increase in the rate, which is common for electrochemical systems and associated with the modulation of faradic currents with increase in sweep rates. Light illumination reduces peak separations for both systems and all sweep rates, which indicates faster kinetics.

For estimation of the HET rate, we employ the Nicholson method,[43,49−52] which involves calculations of the kinetic parameter ψ defined as

$$\psi = k^0[\frac{\pi DnvF}{RT}]^{-1/2} = k^0[0.090434\, Dv]^{-1/2} \quad (3)$$

This parameter ψ[44] can be found from the CV data as

$$\psi = [\frac{-0.6288 + 0.0021X}{1 - 0.017X}] \quad (4)$$

where $X = \Delta E_p$. In Figure 3e,f, the parameter ψ estimated for each sweep rate is plotted as the function of $v^{-1/2}$. According to eq 3, the slope of this dependence $\beta = \frac{\psi}{v^{-1/2}}$ is linearly proportional to the HET rate,

$$\beta = k^0\sqrt{\frac{RT}{DnF\pi}} \quad (5)$$

Estimations for our experiments yield (the indexes indicate the particular case)

$\beta_{dark}^{flat} = 1.05 \pm 0.5\ mV^{1/2}/s^{1/2}$, $\beta_{light}^{flat} = 2 \pm 0.5\ mV^{1/2}/s^{1/2}$
$\beta_{dark}^{nano} = 1.2 \pm 0.15\ mV^{1/2}/s^{1/2}$ and $\beta_{light}^{nano} = 1.4 \pm 0.1\ mV^{1/2}/s^{1/2}$

The diffusion coefficients for $Fe(CN)6^{3-/4-}$ at oxidation and reduction are correspondingly $D_0 = 4.4 \times 10^{-5}$ cm^2/s and $D_R = 5.4 \times 10^{-5}$ cm^2/s at room temperature.[43] Assuming that in dark in both flat and nanostructured systems, all parameters entering eqs 2a−4 are the same, and using $D = 0.5(D_0 + D_R)$, the HET rate in flat gold can be estimated as k_{flat}^{0dark} =0.0024 ± 0.0002 cm/s. The HET rate in nanomesh is in the same range, k_{nano}^{0dark} = 0.0027 ± 0.0002 cm/s.

Under light illumination, the slope β grows almost 2-fold in the flat system (Figure 3e), while in the nanomesh system, the change is not that significant, $\frac{\beta_{light}^{nano}}{\beta_{dark}^{nano}} = \sim 1.2$. Let us take into account that the Nicholson parameter ψ, eq 3, is determined by both the HET rate and charge transport kinetics in the solution, which is assumed to be associated with the diffusion. Let us assume that the kinetic factor that enters eq 1 as $(D/RT)^{1/2}$, and eq 5 as $(D/RT)^{-1/2}$, is changed by light, for example, due to photoinduced heating of the electrode. According to[39,53] for the gold film of 40 nm thick, absorption at 589 nm is 10%, while for gold nanomesh, it is of about 30−40%. Thus, the effects associated with light illumination (for example, photoinduced heating) are expected to be stronger in nanomesh than in flat gold. This is consistent with photoinduced changes in peak currents, which are higher in nanomesh than in flat gold (eqs 2b and a correspondingly).

Combining eqs 1 and 5, photoinduced changes in HET rates can be estimated as

$$\frac{k_{light}^{0flat}}{k_{dark}^{0flat}} = \frac{\beta_{light}^{flat}}{\beta_{dark}^{flat}}\frac{\alpha_{light}^{flat}}{\alpha_{dark}^{flat}} = 3.1 \pm 0.1 \text{ in the flat system} \quad (6a)$$

$$\frac{k_{light}^{0nano}}{k_{dark}^{0nano}} = \frac{\beta_{light}^{nano}}{\beta_{dark}^{nano}}\frac{\alpha_{light}^{nano}}{\alpha_{dark}^{nano}} = 3.2 \pm 0.2 \text{ in the nanomesh system} \quad (6b)$$

Thus, the photoinduced acceleration of electron transfer is significant and is of the same order in both nanostructured and flat gold systems. At the same time, photoinduced changes in peak currents are much stronger in the vicinity of gold nanomesh in comparison with the flat electrode.

Which mechanisms are responsible for modifications of chemical reactions in the nanostructured and plasmonic environment, this is the subject of many scientific discussions. Different models are discussed involving generation of hot electrons,[24−29] modification of surface charges,[39] significant local electric effects[54−56] associated with high optical fields and high gradients of optical fields, and photoinduced heating.[57]

The photoinduced heating can be a factor. Let us roughly estimate possible heating in our experimental conditions. Considering the predominant channel of the heat transfer from the illuminated spot (with the diameter a = 5 mm) to the solution (with the thermal conductivity, c_w = 0.6 W/mK) and then to the cuvette walls (d = 2 cm away). We take into account that at distances $x \ll a$ from the surface, heat flow is mostly perpendicular to the surface, while at larger distances, it becomes isotropic. For a very rough estimation, the thermal resistance can be estimated as

$$R = \int_0^{2a}\frac{dx}{a^2c_w} + \int_{2a}^{d}\frac{dx}{4\pi x^2c_w} \quad (7)$$

Assuming ambient temperature for cuvette walls and the absorbed power with the account of reflection, P = 9.5 mW in the flat gold sample, the estimations yield, $\Delta T = 6.4^0$ in flat gold and up to 3-fold higher in nanomesh. The increased temperature can be partially responsible for accelerated diffusion.[58−61] Commonly, the diffusion does not strongly depend on temperature;[58] however, depending on particular ions and the electrolyte, the effect of heating can be noticeable.[59,61] As an example, in ref 61, the diffusion coefficients of ferrocene/ferricenium in ammonium−imide ionic liquids show 2-fold

https://doi.org/10.1021/acsomega.1c03794
ACS Omega 2021, 6, 34294−34300

increase upon the temperature change from 298 to 323 K, while HET rates change only by 20%.[61]

Our results (in particular, 3-fold change in HET rates) show that the response in charge transport kinetics to the light illumination is stronger than it can be expected solely from the heating. This may indicate a presence of a different mechanism associated with photoexcitation (such as hot electron emission or charging effects). However, note that our rough estimations made above assume a perfect thermal contact between electrodes and the solution. In reality, a temperature difference between the illuminated electrode and solution may result in a significant thermal gradient formed over the double layer; this may be another factor for consideration. Further studies are planned to elucidate the origin of the modifications observed.

CONCLUSIONS

In conclusion, the cyclic voltammetry method is employed to study possible modifications in the electrochemical reaction in a nanostructured plasmonic environment with and without light illumination in the plasmon resonance range. The CV curves are strongly altered under light illumination, and the effect of light on the magnitude of currents is much stronger in the nanostructured system than that in flat gold. The analysis of the charge-transfer rate with the Nicholson method shows that in both systems photoexcitation leads to significant growth of HET rates. Estimations show that effects are stronger than it can be expected solely from the photoinduced heating of the solution.

AUTHOR INFORMATION

Corresponding Author

Mohammad Shahabuddin − *Center for Materials Research, Norfolk State University, Norfolk, Virginia 23504, United States;* orcid.org/0000-0003-4357-3872; Email: m.shahabuddin@spartans.nsu.edu

Authors

Ashleigh K. Wilson − *Center for Materials Research, Norfolk State University, Norfolk, Virginia 23504, United States*

Ashah C. Koech − *Center for Materials Research, Norfolk State University, Norfolk, Virginia 23504, United States*

Natalia Noginova − *Center for Materials Research, Norfolk State University, Norfolk, Virginia 23504, United States*

Complete contact information is available at: https://pubs.acs.org/10.1021/acsomega.1c03794

Notes

The authors declare no competing financial interest.

ACKNOWLEDGMENTS

The work was supported by NSF #1830886, AFOSR FA9550-18-0417, and DoD #W911NF1810472 grants and by the Laboratory Directed Research and Development program at Sandia National Laboratories, a multimission laboratory managed and operated by National Technology and Engineering Solutions of Sandia, LLC, a wholly-owned subsidiary of Honeywell International, Inc., for the U.S. Department of Energy's National Nuclear Security Administration under Contract No. DE-NA-0003525.

REFERENCES

(1) Engheta, N.; Ziolkowski, R. W. *Electromagnetic Metamaterials: Physics and Engineering Explorations*; Wiley, 2006.

(2) Hoffman, A. J.; Alekseyev, L.; Howard, S. S.; Franz, K. J.; Wasserman, D.; Podolskiy, V. A.; Narimanov, E. E.; Sivco, D. L.; Gmachl, C. Negative refraction in semiconductor metamaterials. *Nat. Mater.* **2007**, *6*, 946−950.

(3) Rout, S.; Qi, Z.; Monika, M. B.; Courtwright, D.; Adrien, J. C.; Mills, E.; Shahabuddin, M.; Noginova, N.; Noginov, M. A. Nanoporous gold nanoleaf as tunable metamaterial. *Sci. Rep.* **2021**, *11*, No. 1795.

(4) Belacel, C.; Habert, B.; Bigourdan, F.; Marquier, F.; Hugonin, J. P.; Vasconcellos, S. M. D.; Lafosse, X.; Coolen, L.; Schwob, C.; Javaux, C.; Dubertret, B.; Greffet, J. J.; Senellart, P.; Maitre, A. Controlling Spontaneous Emission with Plasmonic Optical Patch Antennas. *Nano Lett.* **2013**, *13*, 1516−1521.

(5) Noginov, M. A.; Li, H.; Barnakov, Y. A.; Dryden, D.; Nataraj, G.; Zhu, G.; Bonner, C. E.; Mayy, M.; Jacob, Z.; Narimanov, E. E. Controlling spontaneous emission with metamaterials. *Opt. Lett.* **2010**, *35*, 1863−1865.

(6) Li, L.; Wang, W.; Luk, S. L.; Yang, X.; Gao, J. Enhanced Quantum Dot Spontaneous Emission with Multilayer Metamaterial Nanostructures. *ACS Photonics* **2017**, *4*, 501−508.

(7) Noginov, M. A.; Zhu, G.; Mayy, M.; Ritzo, B. A.; Noginova, N.; Podolskiy, V. A. Stimulated Emission of Surface Plasmon Polaritons. *Phys. Rev. Lett.* **2008**, *101*, No. 226806.

(8) Noginov, M. A.; Zhu, G.; Bahoura, M.; Small, C. E.; Davison, C.; Adegoke, J.; et al. Enhancement of Spontaneous and Stimulated Emission of a Rhodamine 6G Dye by an Ag Aggregate. *Phys. Rev. B* **2006**, *74*, No. 184203.

(9) Shubina, T. V.; Toropov, A. A.; Jmerik, V. N.; Kuritsyn, D. I.; Gavrilenko, L. V.; Krasil'nik, Z. F.; Araki, T.; Nanishi, Y.; Gil, B.; Govorov, A. O.; Ivanov, S. V. Plasmon-Induced Purcell Effect in InN/In Metal-Semiconductor Nanocomposites. *Phys. Rev. B* **2010**, *82*, No. 073304.

(10) Noginov, M. A.; Zhu, G.; Bahoura, M.; Adegoke, M. J.; Small, C. E.; et al. Enhancement of Surface Plasmons in an Ag Aggregate by Optical Gain in a Dielectric Medium. *Opt. Lett.* **2006**, *31*, 3022−3024.

(11) Tumkur, T. U.; Kitur, J. K.; Bonner, C. E.; Poddubny, A. N.; Narimanov, E. E.; Noginov, M. A. Control of Forster Energy Transfer in the Vicinity of Metallic Surfaces and Hyperbolic Metamaterials. *Faraday Discuss.* **2015**, *178*, 395−412.

(12) Wubs, M.; Vos, W. L. Forster Resonance Energy Transfer Rate in any Dielectric Nanophotonic Medium with Weak Dispersion. *New J. Phys.* **2016**, *18*, No. 053037.

(13) Ueno, K.; Misawa, H. Surface Plasmon-Enhanced Photochemical Reactions. *J. Photochem. Photobiol., C* **2013**, *15*, 31−52.

(14) Wang, C.; Nie, X. G.; Shi, Y.; Zhou, Y.; Xu, J. J.; Xia, X. H.; Chen, H. Y. Direct Plasmon-Accelerated Electrochemical Reaction on Gold Nanoparticles. *ACS Nano* **2017**, *11*, 5897−5905.

(15) Robatjazi, H.; Bahauddin, S. M.; Doiron, C.; Thomann, I. Direct plasmon-driven photoelectrocatalysis. *Nano Lett.* **2015**, *15*, 6155−6161.

(16) Xu, J.; Gu, P.; Birch, D. J.; Chen, Y. Plasmon-Promoted Electrochemical Oxygen Evolution Catalysis from Gold Decorated MnO_2 Nanosheets under Green Light. *Adv. Funct. Mater.* **2018**, *28*, No. 1801573.

(17) Rasmussen, M.; Serov, A.; Artyushkova, K.; Chen, D.; Rose, T. C.; Atanassov, P.; Harris, J. M.; S Minteer, D. Enhancement of Electrocatalytic Oxidation of Glycerol by Plasmonics. *ChemElectroChem* **2019**, *6*, 241−245.

(18) Wang, C.; Shi, Y.; Yang, D. R.; Xia, X. H. Combining plasmonics and electrochemistry at the nanoscale. *Curr. Opin. Electrochem.* **2018**, *7*, 95−102.

(19) Poddubny, A.; Iorsh, I.; Belov, P.; Kivshar, Y. Hyperbolic metamaterials. *Nat. Photonics* **2013**, *7*, 948−957.

(20) Yao, J.; Liu, Z.; Liu, Y.; Wang, Y.; Sun, C.; Bartal, G.; Stacy, A.; Zhang, X. Optical Negative Refraction in Bulk Metamaterials of Nanowires. *Science* **2008**, *321*, No. 930.

(21) Noginov, M. A.; Barnakov, Y. A.; Zhu, G.; Tumkur, T.; Li, H.; Narimanov, E. E. Bulk photonic metamaterial with hyperbolic dispersion. *Appl. Phys. Lett* **2009**, *94*, No. 151105.

(22) Sheldon, M. T.; Groep, J. V. D.; Brown, A. M.; Polman, A.; Atwater, H. A. Plasmoelectric potentials in metal nanostructures. *Science* **2014**, *346*, 828−831.
(23) Noginova, N.; Rono, V.; Bezares, F. J.; Caldwell, J. D. Plasmon drag effect in metal nanostructures. *New J. Phys* **2013**, *15*, No. 113061.
(24) Linic, S.; Christopher, P.; Ingram, D. B. Plasmonic-Metal Nanostructures for Efficient Conversion of Solar to Chemical Energy. *Nat. Mater.* **2011**, *10*, 911−921.
(25) Brongersma, M. L.; Halas, N. J.; Nordlander, P. PlasmonInduced Hot Carrier Science and Technology. *Nat. Nanotechnol.* **2015**, *10*, 25−34.
(26) Govorov, A. O.; Zhang, H.; Demir, H. V.; Gunko, Y. K. Photogeneration of Hot Plasmonic Electrons with Metal Nanocrystals: Quantum Description and Potential Applications. *Nano Today* **2014**, *9*, 85−101.
(27) Dombi, P.; Hörl, A.; Racz, P.; Marton, I.; Trugler, A.; Krenn, J. R.; Hohenester, U. Ultrafast Strong-Field Photoemission from Plasmonic Nanoparticles. *Nano Lett* **2013**, *13*, 674−678.
(28) Clavero, C. Plasmon-Induced Hot-Electron Generation at Nanoparticle/Metal-Oxide Interfaces for Photovoltaic and Photocatalytic Devices. *Nat. Photonics* **2014**, *8*, 95−103.
(29) Mukherjee, S.; Libisch, F.; Large, N.; Neumann, O.; Brown, L. V.; Cheng, J.; Lassiter, J. B.; Carter, E. A.; Nordlander, P.; Halas, N. J. Hot Electrons Do the Impossible: Plasmon-Induced Dissociation of H_2 on Au. *Nano Lett.* **2013**, *13*, 240−247.
(30) Zhang, Y.; Nelson, T.; Tretiak, S.; Guo, H.; Schatz, G. C. Plasmonic Hot-Carrier-Mediated Tunable Photochemical Reactions. *ACS Nano* **2018**, *12*, 8415−8422.
(31) Gerislioglu, B.; Ahmadivand, A. Functional charge transfer plasmon metadevices. *Research* **2020**, *2020*, No. 9468692.
(32) Yuan, L.; Zhang, C.; Zhang, X.; Lou, M.; Ye, F.; Jacobson, C. R.; Dong, L.; Zhou, L.; Lou, M.; Cheng, Z.; Ajayan, P. M.; Nordlander, P.; Halas, N. J. Photocatalytic Hydrogenation of Graphene Using Pd Nanocones. *Nano Lett.* **2019**, *19*, 4413−4419.
(33) Nayak, S.; Parida, K. M. Dynamics of Charge-Transfer Behavior in a Plasmon-Induced Quasi-Type-II p−n/n−n Dual Heterojunction in $Ag@Ag_3PO_4/g\text{-}C_3N_4$/NiFe LDH Nanocomposites for Photocatalytic Cr(VI) Reduction and Phenol Oxidation. *ACS Omega* **2018**, *3*, 7324−7343.
(34) Piot, A.; Earl, S. K.; Ng, C.; Dligatch, S.; Roberts, A.; Davis, T. J.; Gomez, D. E. Collective excitation of plasmonic hot-spots for enhanced hot charge carrier transfer in metal/semiconductor contacts. *Nanoscale* **2015**, *7*, 8294−8298.
(35) Zeng, P.; Cadusch, J.; Chakraborty, D.; Smith, T. A.; Roberts, A.; Sader, J. E.; Davis, T. J.; Gomez, D. E. Photoinduced electron transfer in the strong coupling regime: waveguide−plasmon polaritons. *Nano Lett* **2016**, *16*, 2651−2656.
(36) Du, L. C.; Furube, A.; Yamamoto, K.; Hara, K.; Katoh, R.; Tachiya, M. Plasmon-induced charge separation and recombination dynamics in Gold-TiO_2 nanoparticle systems: dependence on TiO_2 particle size. *J. Phys. Chem. C* **2009**, *113*, 6454−6462.
(37) Bullock, A.; Clemmons, M.; Shahabuddin, M.; Mashhadi, S.; Yang, C.; Bonner, C. E.; Noginova, N. In *Ultra-Thin Films with Eu3+ Ions for Probing Effects of Local Environment*, Conference on Lasers and Electro-Optics, OSA Terchnical Digest; Optical Society of America, 2018; pp. JTh2A-182.
(38) Xu, T.; Walter, E. C.; Agrawal, A.; Bohn, C.; Velmurugan, J.; Zhu, W.; Lezec, H. J.; Talin, A. A. High-Contrast and Fast Electrochromic Switching Enabled by Plasmonics. *Nat. Commun.* **2016**, *7*, No. 10479.
(39) Shahabuddin, M.; McDowell, T.; Bonner, C. E.; Noginova, N. Enhancement of Electrochromic Polymer Switching in Plasmonic Nanostructured Environment. *ACS Appl. Nano Mater.* **2019**, *2*, 1713−1719.
(40) Lu, W.; Chow, T. H.; Lai, S. N.; Zheng, B.; Wang, J. Electrochemical Switching of Plasmonic Colors Based on Polyaniline-Coated Plasmonic Nanocrystals. *ACS Appl. Mater. Interfaces* **2020**, *12*, 17733−17744.
(41) Agrawal, A.; Susut, C.; Stafford, G.; Bertocci, U.; McMorran, B.; Lezec, H. J.; Talin, A. A. An Integrated Electrochromic Nanoplasmonic Optical Switch. *Nano Lett.* **2011**, *11*, 2774−2778.
(42) Shahabuddin, M.; Noginova, N. *Color Switching of Electrochromic Polymer in Plasmonic Environment*, Metamaterials, Metadevices, and Metasystems; International Society for Optics and Photonic, 2018; Vol. 10719, p. 1071924.
(43) Ameur, Z. O.; Husein, M. M. Electrochemical Behavior of Potassium Ferricyanide in Aqueous and (w/o) Microemulsion Systems in the Presence of Dispersed Nickel Nanoparticles. *Sep. Sci. Technol.* **2013**, *48*, 681−689.
(44) Lavagnini, I.; Antiochia, R.; Magno, F. An Extended Method for the Practical Evaluation of the Standard Rate Constant from Cyclic Voltammetric Data. *Electroanalysis* **2004**, *16*, 505−506.
(45) Khan, A. L.; Sinha, A.; Jain, R. Design, Fabrication, and Optimization of Polypyrrole/Bismuth Oxide Nanocomposite as Voltammetric Sensor for the Electroanalysis of Clofazimine. *J. Electrochem. Soc.* **2018**, *165*, H979−H990.
(46) Zanello, P. *Inorganic Electrochemistry: Theory, Practice and Application*; The Royal Society of Chemistry, 2003.
(47) Elgrishi, N.; Rountree, K. J.; McCarthy, B. D.; Rountree, E. S.; Eisenhart, T. T.; Dempsey, J. L. A Practical Beginner's Guide to Cyclic Voltammetry. *J. Chem. Educ.* **2018**, *95*, 197−206.
(48) Stelling, C.; Singh, C. R.; Karg, M.; König, T. A. F.; Thelakkat, M.; Retsch, M. Plasmonic nanomeshes: their ambivalent role as transparent electrodes in organic solar cells. *Sci. Rep.* **2017**, *7*, No. 42530.
(49) Nicholson, R. S. Theory and Application of Cyclic Voltammetry for Measurement of Electrode Reaction Kinetics. *Anal. Chem.* **1965**, *37*, 1351−1355.
(50) Olmstead, M. L.; Hamilton, R. G.; Nicholson, R. S. Theory of cyclic voltammetry for a dimerization reaction initiated electrochemically. *Anal. Chem.* **1969**, *41*, 260−267.
(51) Muhammad, H.; Tahiri, I. A.; Muhammad, M.; Masood, Z.; Versiani, M. A.; Khaliq, O.; Latif, M.; Hanif, M. A comprehensive heterogeneous electron transfer rate constant evaluation of dissolved oxygen in DMSO at glassy carbon electrode measured by different electrochemical methods. *J. Electroanal. Chem.* **2016**, *775*, 157−162.
(52) Siraj, N.; Grampp, G.; Landgraf, S.; Punyain, K. Cyclic Voltammetric Study of Heterogeneous Electron Transfer Rate Constants of Various Organic Compounds in Ionic liquids: Measurements at Room Temperature. *Z. Phys. Chem.* **2012**, *227*, 105−120.
(53) Gupta, G.; Tanaka, D.; Ito, Y.; Shibata, D.; Shimojo, M.; Furuya, K.; Mitsui, K.; Kajikawa, K. Absorption spectroscopy of gold nanoisland films: optical and structural characterization. *Nanotechnology* **2009**, *20*, No. 025703.
(54) Boerigter, C.; Campana, R.; Morabito, M.; Linic, S. Evidence and implications of direct charge excitation as the dominant mechanism in plasmon-mediated photocatalysis. *Nat. Commun.* **2016**, *7*, No. 10545.
(55) van de Groep, J.; Sheldon, M. T.; Atwater, H. A.; Polman, A. Thermodynamic theory of the plasmoelectric effect. *Sci. Rep.* **2016**, *6*, No. 23283.
(56) Durach, M.; Noginova, N. Spin angular momentum transfer and plasmogalvanic phenomena. *Phys. Rev. B* **2017**, *96*, No. 195411.
(57) Dubi, Y.; Unbc, I. W.; Sivan, Y. Thermal effects - an alternative mechanism for plasmon-assisted photocatalysis. *Chem. Sci.* **2020**, *11*, 5017−5027.
(58) Bahadori, L.; Chakrabarti, M. H.; Manan, N. S. A.; Hashim, M. A.; Mjalli, F. S.; Nashef, I. M. A.; Brandon, N. The Effect of Temperature on Kinetics and Diffusion Coefficients of Metallocene Derivatives in Polyol-Based Deep Eutectic Solvents. *PLoS One* **2015**, *10*, No. e0144235.
(59) Taylor, A. W.; Qiu, F.; Hu, J.; Licence, P.; Walsh, D. A. Heterogeneous electron transfer kinetics at the ionic liquid/metal interface studied using cyclic voltammetry and scanning electrochemical microscopy. *J. Phys. Chem. B* **2008**, *112*, 13292−13299.
(60) Rogers, E. I.; Silvester, D. S.; Poole, D. L.; Aldous, L.; Hardacre, C.; Compton, R. G. Voltammetric Characterization of the Ferrocenel

https://doi.org/10.1021/acsomega.1c03794
ACS Omega 2021, 6, 34294−34300

Ferrocenium and Cobaltocenium Cobaltocene Redox Couples in RTILs. *J. Phys. Chem. C* **2008**, *112*, 2729−2735.
(61) Matsumiya, M.; Terazono, M.; Tokuraku, K. Temperature dependence of kinetics and diffusion coefficients for ferrocene/ferricenium in ammoniumimide ionic liquids. *Electrochim. Acta* **2006**, *51*, 1178−1183.

https://doi.org/10.1021/acsomega.1c03794
ACS Omega 2021, 6, 34294−34300